Atmospheric Research 329 (2026) 108524

Contents lists available at ScienceDirect

Atmospheric Research

journal homepage: www.elsevier.com/locate/atmosres

Rainfall extremes observed by a weather radar in the northern tropical Andes

Sebastián Gómez-Rios [a,*], Alejandro Builes-Jaramillo [a], Hernán D. Salas [b], Juan José Valderrama [a], Juan José Galvis [a]

[a] Institución Universitaria Colegio Mayor de Antioquia, Facultad de Arquitectura e Ingeniería, Medellín, Antioquia, Colombia
[b] Instituto Tecnológico Metropolitano, Facultad de Ciencias Exactas y Aplicadas, Medellín, Antioquia, Colombia

ARTICLE INFO

Dataset link: https://www.siata.gov.co, https://www.copernicus.eu

Keywords:
Precipitation
Extremes
Radar
Orography
Atmospheric environments

ABSTRACT

We characterize seasonal and diurnal spatiotemporal features of extreme rainfall in a 45,000 km^2 area within the tropical Andes of northern South America. We validate radar-based quantitative precipitation estimates for extreme rainfall using in-situ observations, finding a strong spatiotemporal coherence between the datasets through methods based on correlations, timing, and probability mass functions. We then explore the seasonal and diurnal cycles of extreme rainfall, focusing on the local atmospheric environments associated with these extremes. Results show that rainfall extremes in the region (percentile 99.5) exhibit intensities of more than 27 times the average, while the strongest events may reach intensities of up to 85 times the average. Moreover, our findings reveal a consistent timing of extreme precipitation events, occurring between 15:00 and 22:00 LST, accounting at this time range for more than 3% of all seasonal rainfall accumulation. We show that the traditional approach of analyzing seasonal 10-year average rainfall might leave out the high spatiotemporal variability of extreme events. By focusing on a specific threshold and the most intense rainfall events, we identify two main spatiotemporal patterns of extreme rainfall based on the magnitude and the ratio between maxima and mean rain rate. Moreover, these patterns are driven by the interplay of regional atmospheric mechanisms and orographic features. This research improves our understanding about the spatiotemporal characteristics of rainfall extremes and their relationship with atmospheric and orographic factors. It uses high-resolution weather radar data to provide valuable insights for diagnosing, understanding, and modeling extreme rainfall in tropical regions.

1. Introduction

Precipitation is a highly heterogeneous process that constitutes one of the most important climatic variables for the water balance across multiple space and temporal scales (Zoccatelli et al., 2011; Tongal, 2019). Its spatial and temporal distribution governs all hydrological processes. Therefore, investigating its effects on ecosystems on the Earth's surface has become one of the most critical issues in hydrology nowadays (e.g., Liu et al., 2008; Sang et al., 2014; Huang et al., 2014; Shi et al., 2015; Meshram et al., 2017; Raja et al., 2017; Tao et al., 2018).

In general, local hydrometeorological extremes result from the interaction of meteorological systems with local terrain characteristics, such as coasts and orography. Hence, the analysis of these systems that affect extreme precipitation traditionally uses the information generated by meteorological radars at a high resolution.

Marra et al. (2022) analyzed the coastal and orographic effects on the frequency of extreme precipitation in the region covered by a C-band meteorological radar of the Israel Meteorological Service, including rainfall data from 437 daily stations and 65 10 min stations, and spatially adjusting the radar sampling volume with the simplified meta-extreme value method (SMEV). Furthermore, other studies highlight the utility of radar data to characterize extreme flood response in urban watersheds (Villarini et al., 2010) as well as radar data for engineering purposes using Intensity–Duration–Frequency curves (IDF) (Peleg et al., 2018; Srivastava and Mascaro, 2023).

Other studies have addressed extreme precipitation in mid-latitude regions (e.g., Overeem et al., 2009; Wright et al., 2013; Peters and Schumacher, 2015; Dafis et al., 2017). However, there are fewer studies on extreme precipitation events in tropical areas with complex orography, such as the tropical Andes. Espinoza et al. (2015) and Segura et al. (2019) investigated large-scale atmospheric processes that influence extreme rainfall on the eastern slope of the Peruvian Andes. They also studied local and regional scale processes that influence deep convection (the generator of intense precipitation events) in some inter-Andean valleys in Peru. Extreme monthly wet events in the southern

* Corresponding author.
E-mail address: sebastian.gomez@colmayor.edu.com (S. Gómez-Rios).

https://doi.org/10.1016/j.atmosres.2025.108524
Received 5 September 2024; Received in revised form 6 August 2025; Accepted 30 September 2025
Available online 4 October 2025

tropical Andes are related to convection over the western Amazon during the December–March period (Segura et al., 2019). Hernandez-Deckers (2022) has characterized deep convective zones in Colombia and assessed seasonal and diurnal features across different convection hotspots in the country. They highlighted that in some regions of the country, frequent intense convective events can generate heavy rainfall. Poveda et al. (2020) compiled different studies that address high-impact meteorological events throughout the Andes (both in the tropical and extratropical zones). Their work included extreme precipitation events and highlighted, among other aspects, their high spatiotemporal variability due to complex topography and local circulations. They also noted seasonal changes in the diurnal cycle (e.g. Bedoya-Soto et al., 2019) and the influence of mesoscale synoptic processes. Both dynamic and thermodynamic drivers play a role in determining the rainfall patterns across the entire Tropical Andes mountain range, with the upper-level wind being an important driver of rainfall (e.g. Seidel et al., 2019; Villalobos-Puma et al., 2024; Martinez et al., 2024).

In particular, the northwestern Andean region of Colombia is characterized by its highly complex topography, which added to the tropical atmospheric dynamics produces intense atmospheric convection that generates intense or extremely intense precipitation events (e.g., Warner et al., 2003; Poveda et al., 2005; Zuluaga and Houze, 2015; Velásquez, 2022; Gomez-Rios et al., 2023; Hernandez-Deckers, 2022), increasing the hazard of flash floods and landslides in this highly complex topography (e.g. Hoyos et al., 2019; Vega et al., 2024). Additionally, in tropical regions with steep topography, a high spatial and temporal variability of rainfall is observed due to local atmospheric processes, also exerting a strong influence on the development of cloud systems that generate the most intense rainfall (e.g., Espinoza et al., 2015; Chavez and Takahashi, 2017; Poveda et al., 2020; Junquas et al., 2018; Urrea et al., 2019).

Considering the impacts of extreme precipitation events on human communities, the high spatiotemporal variability of precipitation in the Colombian Andes, and the diverse of atmospheric processes influencing the extreme rainfall generation in the northwestern Andean region of Colombia, this study addresses the following questions for the region: (1) Do high spatiotemporal resolution data from a weather radar adequately represent extreme rainfall observations from rain gauges in the Tropical Northern Andes? (2) What are the spatiotemporal patterns of extreme precipitation in the northwestern tropical Andes mountains? (3) What characteristics of the atmospheric environment could be related to extreme precipitation events?

The use of high spatiotemporal resolution observations from a weather radar over a 10-year period provides new insights for the hydrometeorology of the Tropical Andes, given the infrastructure limitations, historical scarcity of in situ data, and gaps in meteorological information.

2. Region of study and datasets

2.1. Study region

This study focuses on a tropical Andes region of northwestern South America (between 5°N/7.5°N - 76.5°W/74.5°W), within a zone that includes two branches of the Andes range (Central and Western ranges) and two main valleys: the Magdalena River Valley (hereafter, Magdalena valley) and Cauca River Valley (hereafter, Cauca valley). Particularly, the Magdalena valley has been previously reported as an area of intense convection (Gomez-Rios et al., 2023; Hernandez-Deckers, 2022). Furthermore, the whole region is also surrounded by areas where intense convective processes drive to heavy rainfall, like the Colombian Pacific coast (Yepes et al., 2019, 2020; Mejía et al., 2021) and the Caribbean lowlands (Zuluaga and Houze, 2015; Albrecht et al., 2016; Liu et al., 2020; Camacho et al., 2022). The region is monitored by a weather radar with a surveillance radius of 120 km located over the Central range, between the Cauca and Magdalena valleys, providing wide coverage over the study region. Fig. 1(a) presents a geographical context of northwestern South America and northern tropical Andes, and Fig. 1(b) provides a zoom into the study region, pointing out the weather radar coverage area and the Cauca and Magdalena rivers.

2.2. Weather radar

We used data on the intensity of rainfall obtained from reflectivity provided by the weather radar of the Metropolitan Area of the Aburrá Valley (AMVA), located at coordinates $6.1913N$, $75.5288W$. This weather radar is a monostatic and pulse-type device with a single directional antenna that emits pulses and receives the responses from the different targets it encounters along the beam path. It is a C-band Doppler-type radar with a magnetron-type transmitter, operating with wavelengths between 4–8 cm with a frequency between 4–8 GHz (Sepulveda, 2016). For Plan Position Indicator (PPI) operations, the radar covers a radius of 120 km (Fig. 1), being used for weather surveillance in northwestern Colombian Andes, including portions of Antioquia, Caldas, Risaralda, and Chocó departments (states). The radar covers portions of the inter-Andean valleys of Magdalena and Cauca rivers, and the Central and Western branches of the Andes range; terrain elevation in the valleys ranges from 125 to 4080 m.a.s.l. Currently, the weather radar is operated by the Environmental Early Warning System of Medellín and the Aburrá Valley (SIATA from its Spanish acronym).

As radar data provides reflectivity, we used radar quantitative precipitation estimates (QPEs) proposed by Sepulveda (2016) for AMVA weather radar reflectivity data. The spatial and temporal resolutions of the reflectivity data are approximately 0.0015^o and 5 min, respectively. To carry out the analysis, the QPEs were resampled to hourly resolution using the mean of the rain rates (mm h^{-1}) recorded within each hour.

2.3. Observational precipitation data

For comparison with radar data, we utilized a rainfall data set consisting of hourly intensity records at 18 rain gauges for the period 2001–2022. These gauges are located in the center and east department of Antioquia on the central range of the Colombian Andes, between the Cauca and Magdalena valleys. The rain gauge stations are scattered around 6.0°N–7.0°N, and 76°W–74.5°W (see Figs. 1(b) and 2(a) and (b)). Rainfall data were provided by Empresas Públicas de Medellín (EPM).

2.4. Reanalysis data

For analyzing regional atmospheric environments, we use ERA5 reanalysis data (Hersbach et al., 2023) at a daily time scale (aggregated from hourly data). In particular, we computed the differences between composites of highest-intensity rainfall events (using the dates of the occurrence as reference) and the 10-year average, for specific humidity, wind speed, and vertical wind speed.

3. Methods

3.1. Validation of radar precipitation data

To identify systematic errors in radar data or precipitation estimates, we compare rain gauge records and QPE (Carr, 2003). To this end, QPE time series are extracted in the same locations of available rain gauge stations. We quantify the Pearson correlation coefficient between QPE and rain gauge time series, and carry out a quantile–quantile (Q-Q) analysis focused on the highest percentiles of rainfall data. In addition, we compute the differences between the empirical cumulative distribution functions (ECDF) of QPE and rain gauge data across the range of rainfall values. We use the maximum difference in

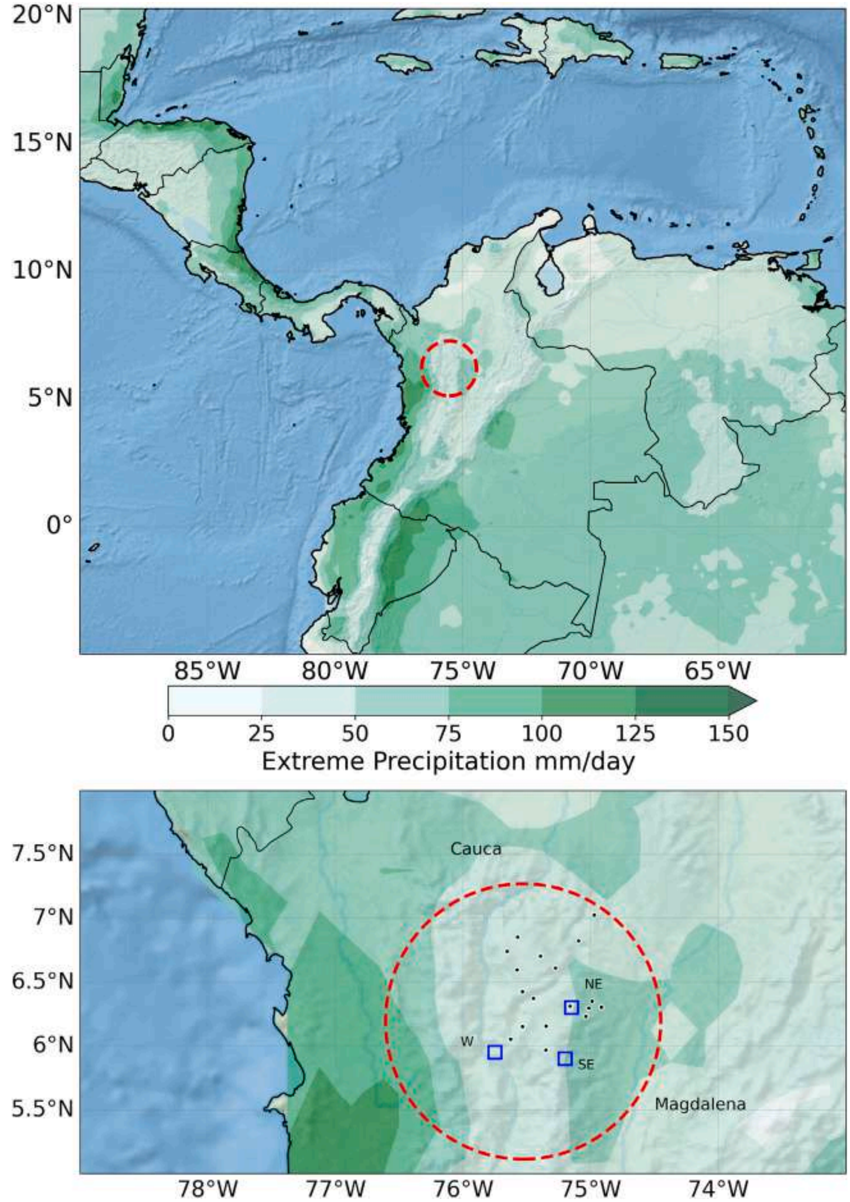

Fig. 1. Study area. (a) Location of the radar coverage in northern South America. The CHIRPS' precipitation 99.5 percentile for the period 2013–2022 is show in green. (b) Radar coverage with the location of rain gauges (black dots) and the regions defined for the analysis (W, NE, SE) (blue boxes).

ECDFs as a measure of the discrepancy between the two probability distributions. The QPE validation includes the rain event scale: for each rain gauge station, the evolution and magnitude of the mean observed rainfall event are compared against the equivalent QPE mean event. In this comparison, an event is a peak in the hourly time series that exceeds 0.13 mm, which is the minimum accumulation consistently measured by the rain gauge. Analogously, we compare the evolution and magnitude of the 100 highest-intensity events in the rain gauge records and the radar data.

3.2. Seasonal and 10-year average extreme rainfall

For 2013–2022, we compute the 10-year and seasonal average rain rate (MAM, JJA, SON, DJF), the standard deviation, and the 99.5th percentile of rainfall intensity (hereafter P99.5) as an index commonly used for extreme precipitation events (e.g. May, 2004; Dave and M.E., 2017; Camuffo et al., 2020). Furthermore, we select the 100 highest-intensity rainfall events for each pixel in the weather radar coverage area, and compute the average rainfall intensity for these events (H100). In addition, we calculate the ratio between P99.5 and the 10-year average rain rate, the ratio between H100 and the 10-year average rain rate, and the corresponding seasonal ratios. This aims to describe the rainfall extremes within the 10-year period and to highlight other possible emerging patterns.

Moreover, three areas of $0.1^\circ \times 0.1^\circ$ stand out for the intensity of extreme events and are defined as follows: (1) the North-Eastern location (NE) is located at the coordinates 6.25°N–6.35°N, 75.2°W–75.1°W, in the foothills of the Andes Central range and western slope of the Magdalena Valley; (2) the South-Eastern location (SE) is located at the coordinates 5.85°N–5.95°N, 75.25°W–75.15°W, also in the foothills of the Central range and the western slope of the Magdalena valley; (3) the Western location (W) is located at 5.9°N–6.0°N, 75.8°W–75.7°W, in the Cauca valley between the Central and Western ranges. More details about the characteristics of these areas are discussed in Section 4.

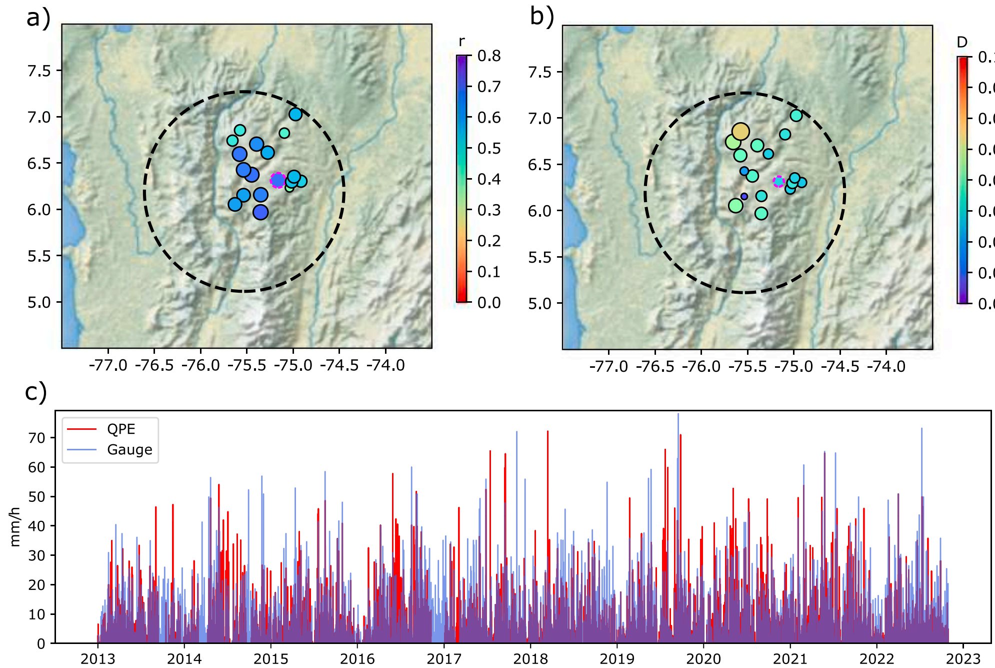

Fig. 2. Validation of radar precipitation data (QPE) compared with observed records in 18 rain gauge stations across the study area. (a) Pearson correlation coefficient between rain gauge time series and QPE time series for the same coordinates. (b) Maximum difference between the empirical CDFs of QPE and rain gauge data in each station. (c) Time series of 2308505 Alejandría rain gauge (transparent blue) and time series of QPE (red) at the same location (6.3129°N, 75.1624°W). Location of the Alejandria gauge is highlighted in panels (a) and (b) with a dashed magenta mark.

3.3. Composite analysis

For NE, SE, and W, we extract the dates associated with events equal to or exceeding P99.5 in each season. We compute the daily average composites for the zonal and meridional wind components, vertical wind speed, and specific humidity on the dates of occurrence of those events. To this end, we consider the difference between the time reported by the weather radar data and the ERA5 datasets. The rainfall event is assigned to the same UTC day if it occurred between 12:00 and 23:59, or to the previous day if it occurred between 00:00 and 11:59. We then compute the daily average.

4. Results and discussion

4.1. Validation of radar precipitation data and extreme events distribution

Fig. 2(a) shows Pearson's correlation coefficient of around 0.7 between precipitation from radar (QPE) and observations for most of the gauge stations, which indicates a good correspondence between both datasets. In addition, Fig. 2(b) shows that, for most stations, the maximum probability difference between the ECDFs of QPE and rain gauge data, aligned by rainfall values, is less than 0.07 (dimensionless). A value of 0 would indicate perfect agreement between the two distributions, while values closer to 1 reflect greater divergence. Therefore, these values suggest that radar and gauge precipitation distributions are reasonably similar. Fig. 2(c) shows consistency in variability and magnitude between the time series of the rain gauge *Alejandria* and the time series from the radar precipitation at the same coordinates.

Fig. 3(a) shows consistency in the mean values of rainfall events, with both QPE and gauge data coinciding at the peak (around 7.35 mm h^{-1}) and capturing the average evolution of the event from 4 h before to 4 h after the rainfall maximum. In terms of standard deviation around the mean, QPE and gauge data align better before and at the peak, although slightly higher deviations are observed in QPE after the rainfall peak. Error bars representing the interquartile range (IQR) indicate greater dispersion in radar estimates, except at the peak; at the 0-hour lag, the 75th percentiles are similar, with slightly higher values for the gauge data. Fig. 3(b) presents a similar comparison for the 100 most extreme events at the station. In this case, the peaks also coincide in their mean value (around 40 mm h^{-1}), and the mean plus standard deviation shows good agreement. The IQR is wider in gauge data before the peak, while higher dispersion is seen in radar estimates after the peak. These analyses indicate that, despite differences related to the nature of the data sources, the two datasets agree in both magnitude and evolution of rainfall events.

Regarding the QPE distribution, Fig. 3(c) shows the probability density of the spatially averaged rain rate in the three selected locations (NE, SE, and W). In particular, NE and SE exhibit lower density values at low rain rates compared to W, while the two eastern locations show higher density values at higher rain rates. NE and SE display similar behavior, although SE shows slightly higher densities at the end of the distribution. Fig. 3(d) also shows consistency between both distributions at the highest percentiles for the rain gauge *Alejandria*, with a slight underestimation of the highest rain rates and a slight overestimation of the lowest rain rates. Event-scale, dispersion, and Q-Q plot analyses were conducted for all stations, and the results show consistency in all rain gauges (not shown).

4.2. 10-Year average rainfall intensity patterns

Fig. 4(a) shows the 10-year average rainfall intensity over the study region, including no-rain periods in its computation. The mean rainfall intensity varies from 0.2 mm h^{-1} to 0.89 mm h^{-1}, with the highest values occurring in two of the selected locations: NE and SE. NE exhibits rainfall intensities around 0.59 – 0.79 mm h^{-1}, and SE shows rainfall intensities in the range 0.79–0.89 mm h^{-1}. In the western portion of the study area, W shows rainfall intensities around 0.39–0.59 mm h^{-1}. The areas with the highest 10-year average (above 0.8 mm h^{-1}) coincide with the 1800 m.a.s.l contour and with topographic hollows over the eastern slopes of the Central range. In particular, elevations around 1800 m altitude have been identified as the pluviometric optimum (PO) in the Colombian Andes, which is characterized by a maximum in

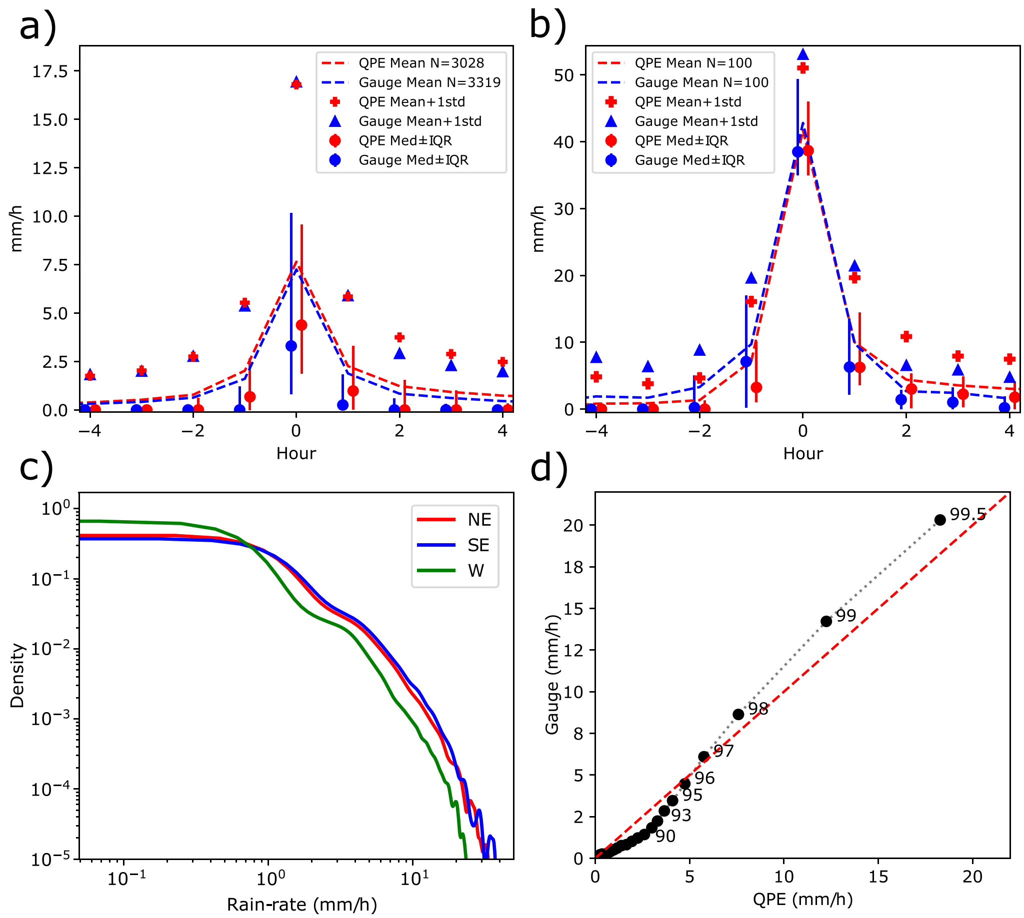

Fig. 3. (a) QPE and rain gauge mean (dashed lines), interquartile range (error bars), and mean plus standard deviation (cross and triangle markers) of typical rainfall events at the Alejandría station, considering time lags from −4 to +4 h.(b) Same as panel (a), but for the 100 most extreme events. (c) Probability density distribution of QPE for the spatially averaged rain-rate in NE (red), SE (blue) and W (green) locations; Both axes are in logarithmic scale. (d) Quantile–Quantile plot for rain gauge and QPE data in the station Alejandría focused on the highest percentiles.

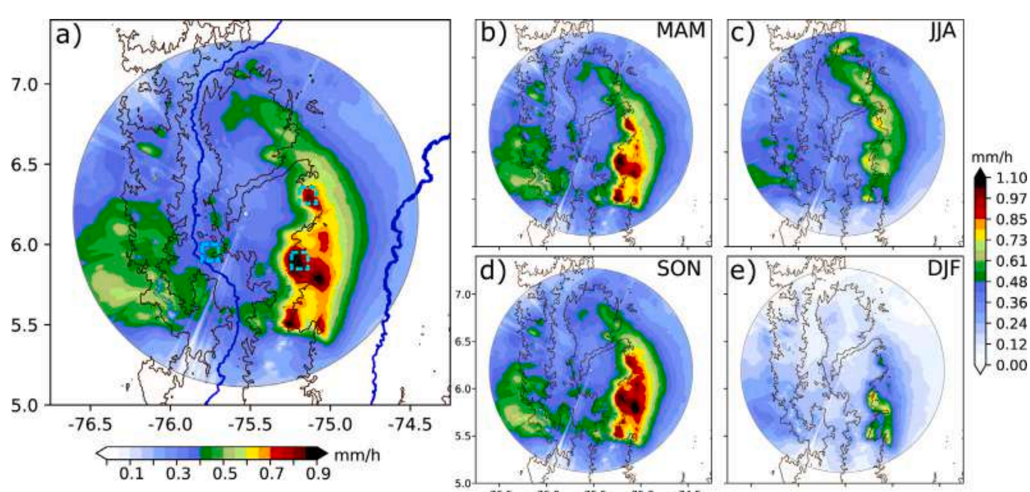

Fig. 4. (a) 10-year average and (b–e) seasonal mean rainfall intensity (mm h^{-1}) patterns. The dark brown contour line is 1800 m.a.s.l. elevation. Dark blue lines denote the Magdalena (east) and Cauca (west) rivers. Cyan boxes are for NE, SE, and W, included in panel (a) for reference.

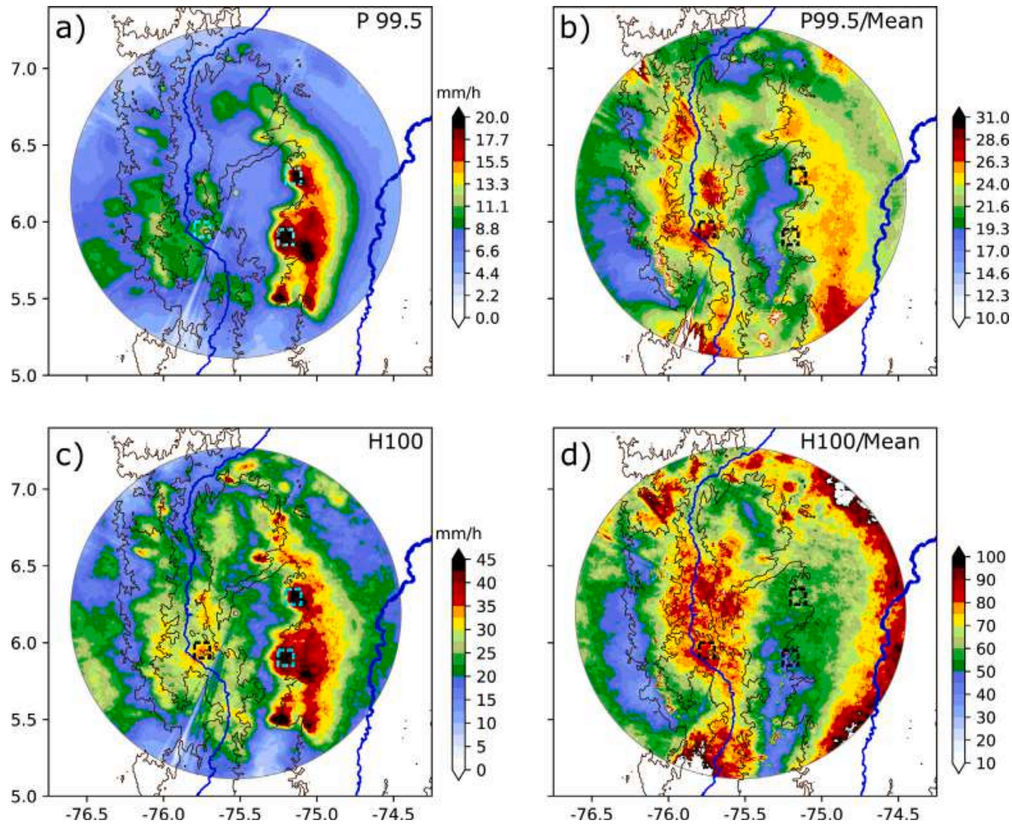

Fig. 5. Spatial patterns of (a) 99.5 percentile (mm h^{-1}), (b) ratio between P99.5 and the mean rain-rate (dimensionless), (c) average of the 100 highest-intensity rainfall events (mm h^{-1}), and (d) ratio between the average of 100 highest-intensity rainfall events and the 10-year mean rain-rate (dimensionless). Cyan and black boxes are NE, SE, and W locations.

annual precipitation, a reduction of precipitation upwards related to decreased humidity with altitude, and a reduction downwards associated with less evaporative input (Oster, 1979; Arias et al., 2021).

Figs. 4(b–e) shows the seasonal patterns of rainfall intensity, in agreement with previous results (e.g. Urrea et al., 2019), exhibiting that the main 10-year average patterns remain similar during the wet seasons (MAM and SON), while during dry seasons (JJA and DJF) there is a contrasting behavior. In particular, during DJF, rainfall exhibits the lowest values across the study area, reaching intensities of up to 0.50 mm h^{-1}, whereas during JJA, rainfall patterns in the east remain similar to those of the wet seasons but with lower rain intensity, ranging between 0.48 – 0.80 mm h^{-1} at the eastern and northern foothills. For dry seasons, the southwestern rainfall intensity pattern is not evident.

4.3. Patterns of rainfall extremes

Fig. 5 shows the spatial patterns for P99.5, H100, the ratio between P99.5 and the 10-year average rainfall, as well as the ratio between H100 and the 10-year average rain rate.

Fig. 5(a) shows that the highest P99.5 values are located in the eastern foothills of the Central range, similar to the 10-year average rainfall (Fig. 4(a)), and coinciding with NE and SE locations. Analogous to 10-year average rainfall, areas with the highest P99.5 values in the Magdalena Valley (20 mm h^{-1}) coincide with the 1800 m.a.s.l contour and some topographic hollows. Also, there are areas in the Cauca valley (e.g. W) where P99.5 values exceed those in most of the western portion of the study area, reaching around 12 mm h^{-1}. The Cauca Valley shows lower P99.5 values than the Magdalena Valley, although rainfall intensity extremes relative to the mean are notable in this region (Figs. 5(b) and (d)). In this sense, several areas along the Cauca Valley exhibit that P99.5 is more than 27 times the mean intensity of rain (e.g. W).

The spatial distribution of H100 (Fig. 5(c)) resembles the spatial distribution of P99.5, but with some differences, especially in the Cauca valley and in the western half of the study area. Close to 6°N in the Cauca valley (W), there are areas where H100 is comparable in magnitude to some areas on the eastern slope of the Central range (e.g. SE and NE), despite the Cauca valley having smaller values of P99.5. Also, the H100 spatial patterns exhibit several rain rate peaks over topographic hollows, especially around the Central Range.

For the ratio between H100 and the mean rain rate, the contrast between the eastern slopes of the Central range and the floor of the valleys becomes more pronounced. In the Cauca valley, H100 is around 85 times the mean rain rate (Fig. 4(a)), while the slope facing the Magdalena Valley exhibits H100 values around 60 times the mean rain rate (Fig. 4(a)). The Magdalena Valley bottom also shows high values of the H100/mean ratio, but its location on the border of the radar coverage area reduces the reliability of this pattern.

4.4. Seasonal and diurnal patterns of rainfall extremes

Extreme rainfall variability exhibits seasonal changes in the magnitude and location of these extremes. The spatial distribution of P99.5 during each season is shown in Fig. 6. During the wet seasons MAM and SON (Figs. 6(a) and (c)), we found that the distinctive pattern found for the 10-year average persists over NE, SE, W, and around the 1800 m.a.s.l. and topographic hollows. For those two seasons, the rainfall intensity over the Magdalena valley slopes is around 20 mm h^{-1}. For the dry seasons JJA and DJF, P99.5 exhibits a high intensity in NE and SE, with two particularities for JJA: (i) the extreme intensity pattern goes further north, and (ii) evidence of high intensities is also observed above W. The seasonal and 10-year average results show a pattern of higher rainfall intensity at altitudes around 1800 m.a.s.l. and also in the topographic hollows of the Magdalena valley and Cauca

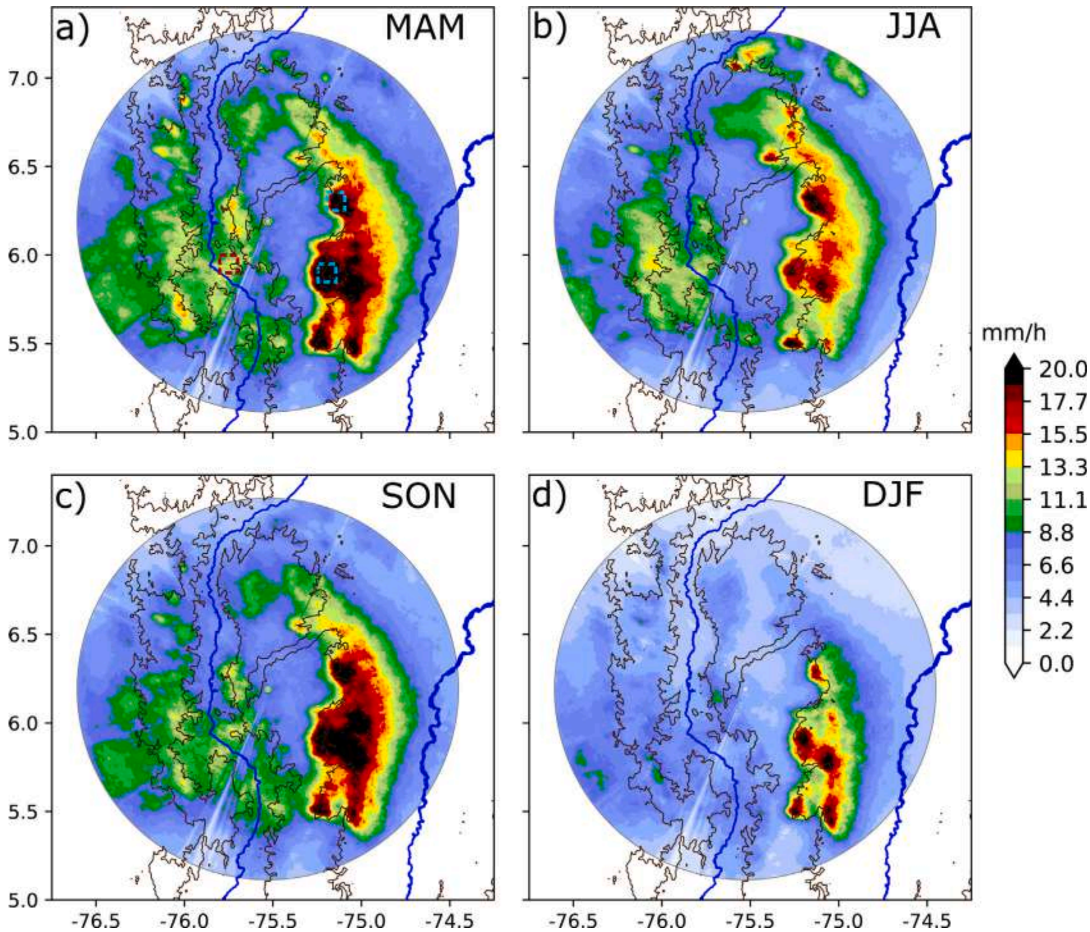

Fig. 6. Seasonal patterns of percentile 99.5 of rainfall intensity (mm h^{-1}). The dark brown contour is for 1800 m.a.s.l. altitude. Dark blue lines are Magdalena (east) and Cauca (west) rivers, included in panel (a) for reference. The boxes for NE, SE, and W are included in cyan and red for reference in (a).

valley slopes. Similar features are also found for P99.5 and the highest 100 events in MAM and JJA (Figs. 7(a) and (b)).

The ratio of P99.5 to the mean rain rate for MAM highlights areas in the Cauca valley where events are up to 28 times stronger than average (Fig. 7(c)); regarding the H100 to mean ratio and, MAM displays widespread areas in the Cauca valley where H100 is more than 43 times the average rain rate (Fig. 7(e)). Notably, in the same valley and for the JJA season, there is an area near 5.9N where H100 reaches intensities around 60 times the average rain rate (Fig. 7(f)). Although there are other zones where the H100/mean ratio is higher than 65 (south), these zones are located on the border of the radar coverage area, where uncertainty is greater.

Fig. 8 illustrates the diurnal cycles of hourly accumulated rainfall associated with P99.5 events for each season (a, c, and e panels) and the percentage of total seasonal accumulations represented by these events (b, d, and d panels) in the NE, SE, and W locations. For rainfall accumulation due to extreme events, the absolute magnitude in NE and SE differs from that in W. NE and SE locations exhibit peaks around 500 mm in the evening around 20:00 LST and 20:00–22:00 LST, respectively, while W shows peaks around 200 mm with an earlier occurrence (15:00–20:00 LST). Moreover, for the three locations, the percentage of rainfall accumulation around the peak can reach approximately 3% of the total seasonal accumulation during DJF (W), DJF-MAM-JJA (NE), and JJA (SE).

The timing of extreme rainfall in NE and SE coincides with findings by Hernandez-Deckers (2022) regarding deep convection in the area. He showed that the western slope of the middle Magdalena Valley around 6N experiences a high frequency of deep convective events starting from 20:00 LST; further north, around 7N, high frequencies begin earlier, from 18:00 LST. He also noted that the peak of deep convection on the valley floor occurs mainly around midnight. In this sense, Gómez-Ríos et al. (2019) pointed out that during 2014–2016, in the time range 15:00–21:00 LST the deep convective cells mainly developed in the foothills of the Magdalena Valley whereas the wide convective cells in that area were more frequent around midnight.

Spatial patterns of rainfall intensity suggest that the slopes of the Magdalena Valley stand out due to their high absolute extremes whereas the Cauca valley is notable for its extreme events when compared to the 10-year average rainfall. Moreover, the location and intensity of these rainfall extremes exhibit seasonal changes. Despite the geographic closeness of the Cauca and Magdalena Valleys (less than 100 km), the complex orography imposes differences in the regional and local processes, which contribute to identifying the extreme rainfall patterns.

4.5. *Atmospheric environments associated with the extreme rainfall intensity*

In order to uncover aspects of the atmospheric environments surrounding extreme events during MAM and JJA, we computed the average fields of specific humidity (SH) and winds for the P99.5 event dates, as well as the 10-year seasonal mean in these variables, at 850 hPa and 500 hPa (Figs. 9 and 10). In addition, differences between them were calculated.

During MAM, at 850 hPa (Fig. 9 bottom panels), the study region exhibits low-level wind convergence of westerly, northeasterly, and southeasterly winds around the Central-Western Andes. This horizontal convergence is still present during the extreme events, while an

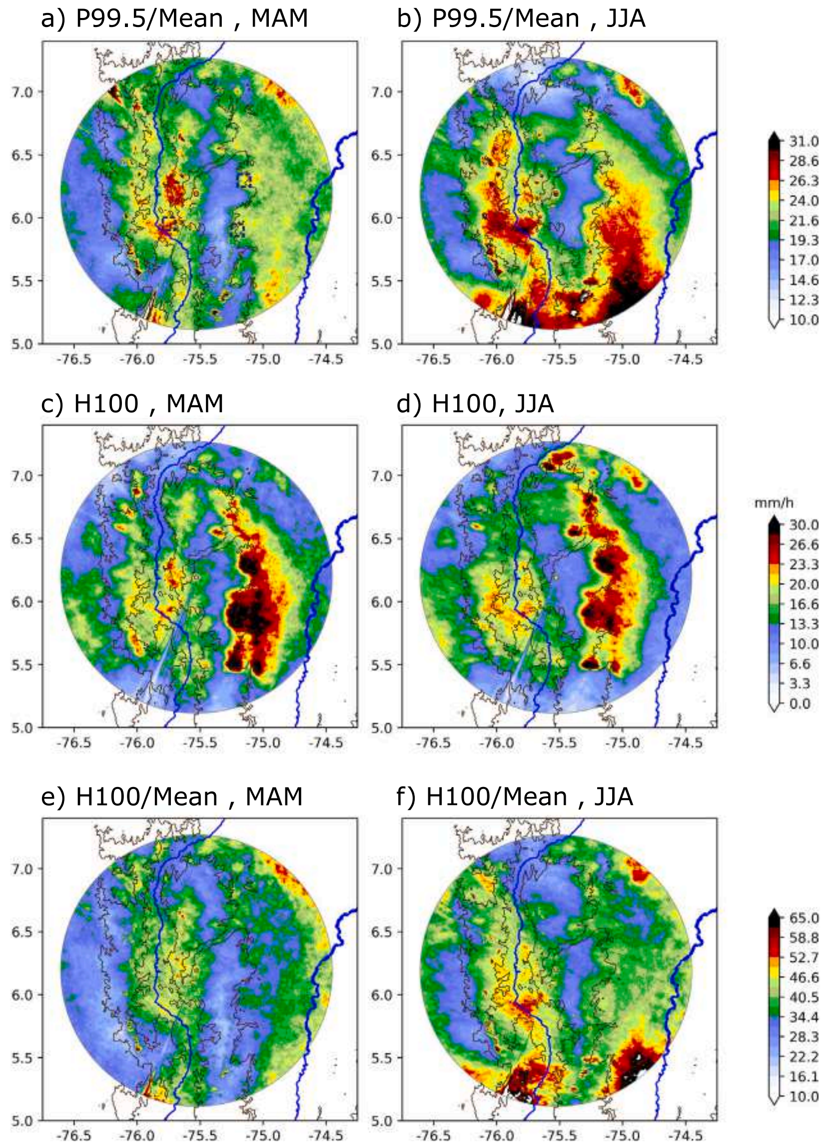

Fig. 7. Spatial patterns for H100 (mm h^{-1}) for (a) MAM and (b) JJA. Spatial patterns of the ratio between P99.5 and mean for seasons (a) MAM and (b) JJA. Spatial patterns of the ratio between H100 and mean for (e) MAM and (f) JJA. The boxes for NE, SE, and W are included in black for reference in (c).

increase in SH is found in the north, northeast, and western parts of the study area. Possibly, the higher availability of water vapor favors the formation of precipitating systems, which are enhanced convergence near the foothills of the range and ascent around the terrain features.

Interestingly, around the SE region, extremes are associated with a decrease in SH; this is related to a strengthening of dry down-valley (southerly) winds from the High Magdalena basin, possibly influenced by the Orinoco LLJ through the gap at 3.5°N 75°W (Vásquez-Franco et al., 2023). Despite the lower content of moisture in this down-valley flow, its strengthening could favor low-level (Fig. 9, 850 hPa) wind convergence between 5.5°N and 6.5°N and enhance the moist convection in the eastern portion of the study region (Gomez-Rios et al., 2023). At middle levels (Fig. 9, 500 hPa), the strengthening of easterlies appears to supply moisture that helps sustain the deep convection that triggers the extreme rainfall events.

During JJA extreme rainfall events, there is a weakening of the low-level flow in the Magdalena Valley that may favor the advection of moisture from the north and northeast, resulting in an increase in SH on the eastern side of the study area and convergence, particularly along the western slopes of the Central Andes (Fig. 9, 850 hPa). Differences in vertical velocity fields (not shown) indicate enhanced upward motion in the same region where increased SH and low-level wind convergence are observed. At mid-levels (Fig. 9, 500 hPa), easterly winds on dates of extreme rainfall are moister and weaker than the seasonal mean state.

These results indicate changes in the low-level flow along the Magdalena Valley and the mid-level zonal circulation that can be associated with P99.5 events over the eastern side of the radar coverage (SE and NE locations). The intensification of southerly downvalley flow during MAM and weakening during JJA seem to promote convergence over the eastern foothills of the Central Andes, which weather radar identifies out the areas of extreme rainfall intensity. The role of the Magdalena wind system in precipitation and convection has been highlighted by previous works (e.g., Gomez-Rios et al., 2023; Velásquez, 2022; Camacho et al., 2022; Bohórquez and Hernández-Deckers, 2023). At middle levels, easterlies prevail in both seasons with intensification during MAM. Such winds may advect more moisture, helping sustain the convective events that generate extreme rainfall.

According to Zuluaga and Houze (2015), deep convective cores in JJA are linked to a diurnal gradient in geopotential height fields that promotes onshore flow and convergence along the northeastern Andes in the late afternoon. Additionally, the low-level circulation around the mountains (Fig. 10, 850 hPa), centered near 7°N, 77°W, might

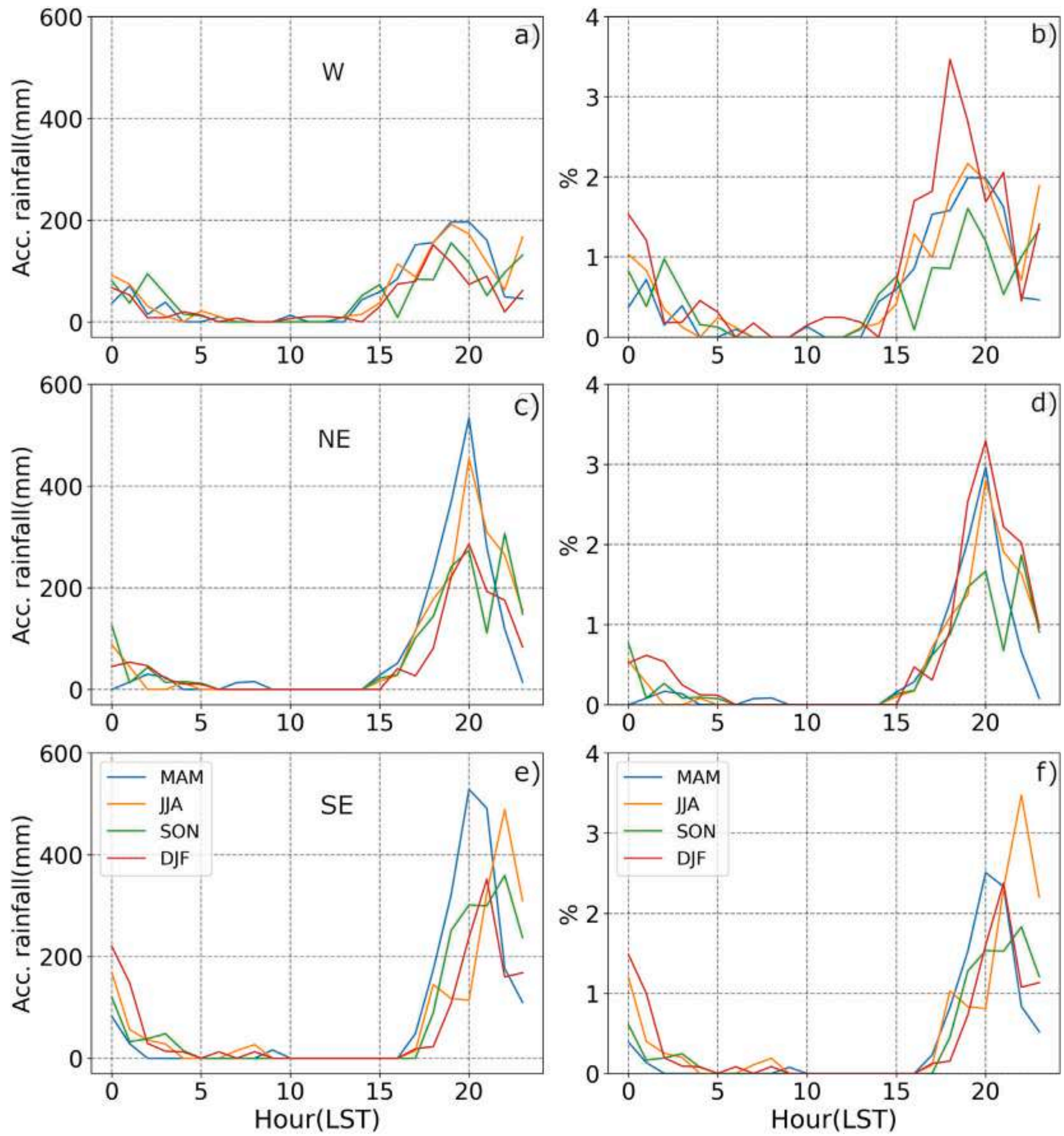

Fig. 8. Diurnal cycle of hourly accumulated rainfall for events over the P99.5 percentile in each season (a, c, and d) and the percentage of the total seasonal accumulations represented by these events (b, d, and e) in the NE, SE, and W locations.

be associated with a clockwise turn of the Caribbean Low-Level Jet over northern Colombia (Robledo et al., 2024). The strengthening and displacement of this clockwise circulation could also influence the wind change in the northern Magdalena Valley.

The weakening of winds during JJA may help retain moisture at the mid-levels in the region and could reduce the shear that might disorganize the precipitating systems triggered in the foothills. Nevertheless, more research is needed regarding the role of vertical shear.

Regarding the W location, the local-scale processes that govern the P99.5 events could be out of the ERA5 resolution. Therefore, further efforts (such as regional modeling) are needed to explain the extreme features of rainfall found from the radar QPE information.

5. Final remarks and future work

Weather radar datasets offer high spatiotemporal resolution observations at short-term extreme precipitation. This is fundamental for advancing their characterization and understanding (Lengfeld et al., 2020; Eldardiry and Habib, 2020), despite the challenges regarding short radar-record length and uncertainty in radar-based quantitative precipitation estimation (QPE), and possible limitations due to the definition of extreme events (Zwiers et al., 2013). In this work, we found agreement between rain-gauge observations and QPE for the continuous time series and also for data points above the 90th percentile.

Although several works have studied extreme rainfall variability using different approaches (e.g., Raymond et al., 2020; Kuswanto et al., 2015; Stott et al., 2016; Schär et al., 2016), we found that rainfall extremes in this northern Andean region can be characterized with two predominant patterns: (i) one based on the magnitude of extreme rainfall intensity and (ii) another based on the ratio between the rainfall intensity and mean rain rate. When analyzed in terms of magnitude, rainfall extremes are most intense in the Magdalena Valley and along the foothills of the Central Andes range, located in the eastern portion of the study area. When extreme rainfall is compared to the mean, the Cauca Valley stands out as an area where extreme rainfall is considerably strong relative to the mean rain rate. These patterns highlight the SE, NE, and W locations as hotspots of extreme rainfall.

Our findings suggest that the most intense rainfall events occur in the MAM and SON trimesters, which are the wet seasons in the northern Andes (Urrea et al., 2019). Among the dry seasons, JJA exhibits higher values of extreme precipitation. Furthermore, there is a consistent

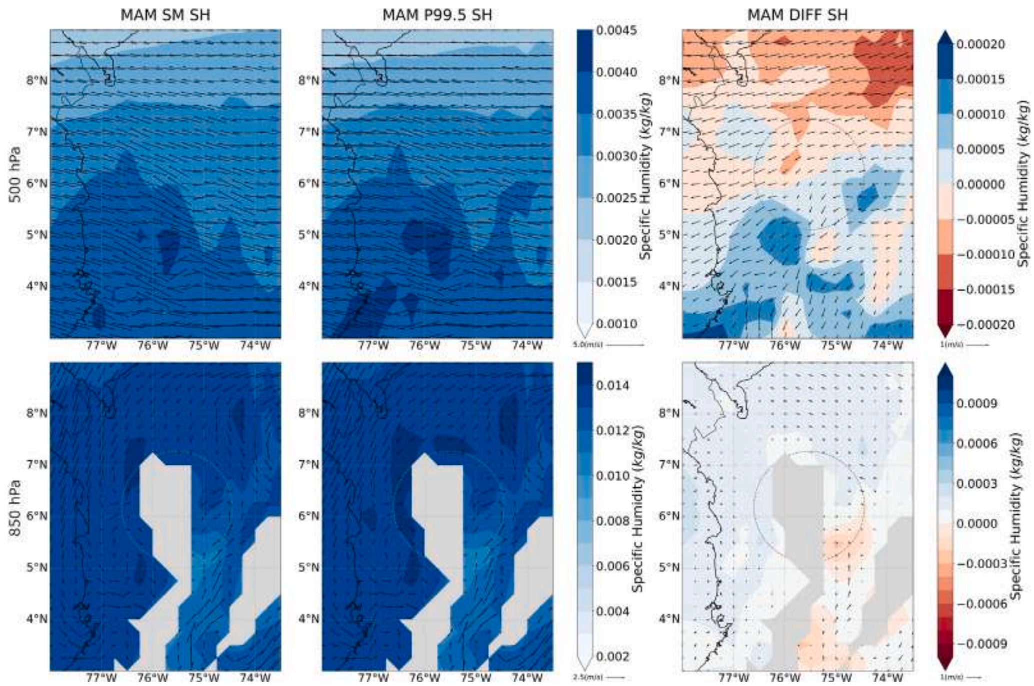

Fig. 9. Specific humidity and wind composites for 500 hPa and 850 hPa during MAM. Seasonal mean (left), Extreme Events Mean (center) and, Difference between Extreme Events Mean and Seasonal mean (right). Gray areas in the lower panels depict heights above 1500 m.a.s.l.

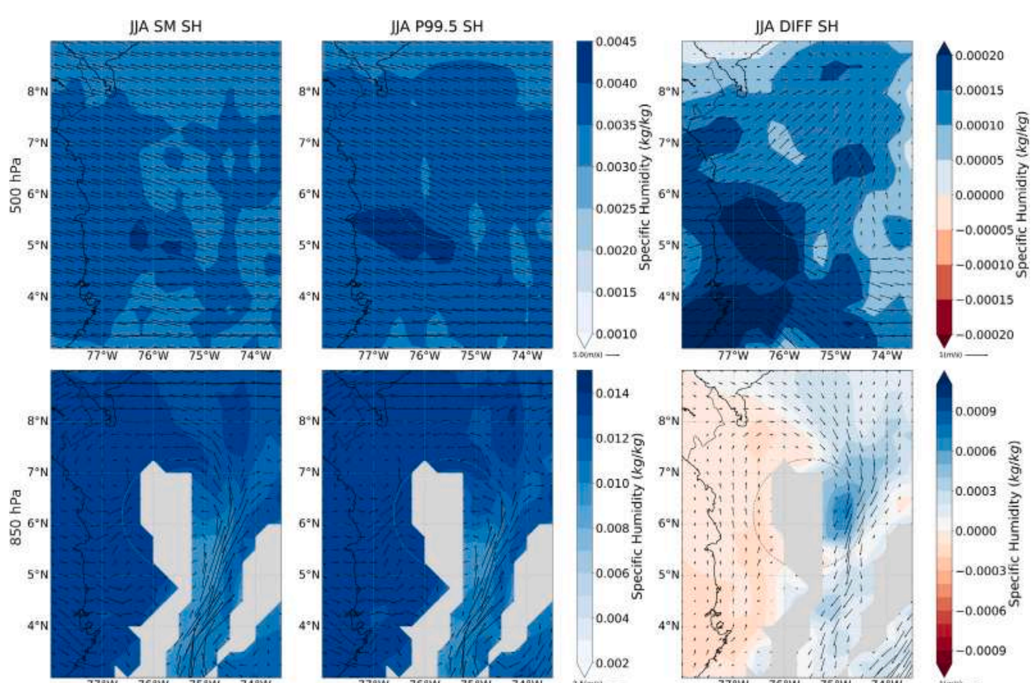

Fig. 10. Same as Fig. 9 for JJA.

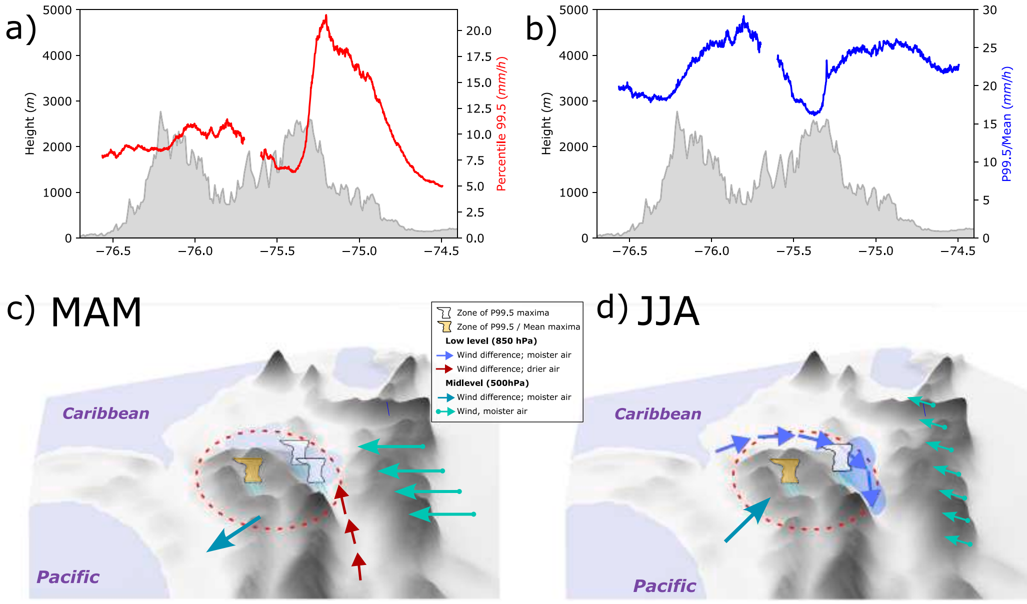

Fig. 11. Cross sections of the Central and Western Andes ranges at 5.9°N for (a) P99.5 of rain rate and (b) P99.5 relative to the mean rain rate. Schematics of relevant seasonal dynamic patterns related to extreme rainfall in the region during (c) MAM and (d) JJA. Red and dark blue arrows are for seasonal differences (extreme events minus mean state) in low-level wind, with color indicating a decrease (red) or increase (blue) in specific humidity (SH). Light cyan tailed arrows represent wind at middle levels (500 hPa) and positive seasonal differences of SH, while dark cyan arrows represent wind differences and increases in SH at the same level. Indicative locations of the maxima of P99.5 and P99.5 relative to the mean are also included.

timing of extreme events throughout the year, which provides valuable insights for diagnosis, predictive modeling, planning, and disaster risk management.

Our results indicate that extreme events typically occur between late afternoon and early evening across the SE, NE, and W locations during all seasons. For a more detailed seasonal analysis, we focused on the MAM wet season and the JJA dry season. Although extreme events occur at similar times, the physical precursors appear to differ between MAM (wet) and JJA (dry) seasons. This suggests that varying interactions among hydrometeorological variables may influence the formation and development of these extremes, leading to differences in the spatial distribution of extreme rainfall patterns.

Extremes in MAM appear to develop in an atmospheric environment with strengthened and moister easterlies at middle levels and an enhanced southerly downvalley wind at low levels, in contrast to JJA, when extreme rainfall seems to develop in weaker but moister easterlies and enhanced northerly flow in the Magdalena Valley. However, detailed analyses of interactions with valley features, hillslopes, and finer-scale processes are necessary for a more comprehensive understanding of the identified extreme patterns.

In order to highlight the relevance of the terrain features in extreme precipitation, Figs. 11(a) and (b) show cross sections of the Central and Western Andes at 5.9°N, with P99.5 and P99.5 relative to the mean. The of P99.5 maxima stand out to the east, in the foothills of the Central Andes and the Magdalena Valley, and the high P99.5 values in the Cauca Valley (west) are notable when they are compared relative to the mean. Furthermore, Fig. 11 summarizes some of the aforementioned seasonal patterns around extreme precipitation events.

While our findings highlight important spatial patterns, we recommend validating these results using higher-resolution datasets, given the known limitations of the coarse ERA5 reanalysis in capturing regional and local climate features in complex topographies (Mutlu, 2025; Kara and Elbir, 2025; Wei et al., 2025; Hu and Yuan, 2021). Extended regional convection-permitting modeling efforts can greatly improve our understanding of the local dynamics and thermodynamical processes that lead to extreme rainfall events in complex topographic areas like the tropical northern Andes. For northwestern South America, studies such as Gomez-Rios et al. (2023), Hernandez et al. (2024), Martinez et al. (2024) addressed convection-permitting modeling focused on specific events or periods (several weeks or a couple of months). 10-year average convection-permitting simulations (e.g., Dominguez et al., 2024) would provide more insights into the reasons behind the higher frequency of extreme events in certain locations of the inter-Andean valleys, and further elucidate the processes that influence the different extreme rainfall patterns identified in this work.

Moreover, this work opens new avenues for future research, such as: (i) Along the Andes mountains of Colombia, mean precipitation exhibits a pluviometric optimum (PO) (e.g. Arias et al., 2021; Oster, 1979). Is the PO also a feature of rainfall extremes? (ii) Considering that radar QPEs can be useful for operational intensity–duration–frequency (IDF) curves in regions monitored by weather radars (Srivastava and Mascaro, 2023), what are the spatial patterns of IDF from radar QPEs in the region? (iii) can convection-permitting simulations adequately capture the characteristics of extreme events and provide detailed information about the dynamics behind their occurrence in a tropical area of complex terrain? (iv) What is the relationship between the timing and magnitude of rainfall extremes and Mesoscale Convective Systems in the study region?; (v) How could changes in vertical shear be related to the occurrence of extreme rainfall events in the tropical Andes.

CRediT authorship contribution statement

Sebastián Gómez-Rios: Writing – original draft, Software, Data curation, Conceptualization. **Alejandro Builes-Jaramillo:** Writing – original draft, Methodology, Data curation, Conceptualization. **Hernán D. Salas:** Writing – original draft, Methodology, Conceptualization. **Juan José Valderrama:** Data curation. **Juan José Galvis:** Data curation.

Declaration of competing interest

The authors declare that they have no known competing financial interests or personal relationships that could have appeared to influence the work reported in this paper.

Acknowledgments

The work of S. Gómez-Ríos, A. Builes-Jaramillo, J. J. Valderrama, and J. J. Galvis was supported by Institución Universitaria Colegio Mayor de Antioquia (project FAI118). The work of H. D. Salas was supported by the Institución Universitaria Colegio Mayor de Antioquia (project FAI118) and the Instituto Tecnológico Metropolitano, project NFRFI-2023-00561 funded by the Government of Canada's New Frontiers in Research Fund (NFRF), attributed to the Natural Sciences and Engineering Research Council of Canada (NSERC) and the Social Sciences and Humanities Research Council of Canada (SSHRC). We thank Empresas Públicas de Medellín (EPM) for access to the rainfall data; Sistema de Alerta Temprana del Valle de Aburrá (SIATA) for weather radar data, especially to J. Sepúlveda for his diligence regarding data curation and availability; and European Copernicus Programme for ERA5 Reanalysis data is available at the website (https://www.copernicus.eu/).

Data availability

Radar weather data will be made available on request to SIATA through the web page https://www.siata.gov.co or via email contacto@siata.gov.co. Rain gauge data is available upon request to Empresas Públicas de Medellín via email epm@epm.com.co. ERA5 Reanalysis data is available at the European Copernicus Programme website https://www.copernicus.eu.

References

Albrecht, R.I., Goodman, S.J., Buechler, D.E., Blakeslee, R.J., Christian, H.J., 2016. Where are the lightning hotspots on earth? Bull. Am. Meteorol. Soc. 97 (11), 2051–2068.

Arias, P.A., Garreaud, R., Poveda, G., Espinoza, J.C., Molina-Carpio, J., Masiokas, M., Viale, M., Scaff, L., van Oevelen, P.J., 2021. Hydroclimate of the andes part II: Hydroclimate variability and sub-continental patterns. Front. Earth Sci. 8, http://dx.doi.org/10.3389/feart.2020.505467, URL: https://www.frontiersin.org/articles/10.3389/feart.2020.505467.

Bedoya-Soto, J.M., Aristizábal, E., Carmona, A.M., Poveda, G., 2019. Seasonal shift of the diurnal cycle of rainfall over Medellin's valley, central andes of Colombia (1998–2005). Front. Earth Sci. 7, http://dx.doi.org/10.3389/feart.2019.00092.

Bohórquez, C., Hernández-Deckers, D., 2023. Caracterización de la convección atmosférica nocturna en el Magdalena Medio (M.Sc. Thesis). Universidad Nacional de Colombia, Medellín Colombia.

Camacho, J., Martinez, J., Arias, P., 2022. Sistemas Convectivos de Mesoescala: una visión desde las simulaciones de Convección Permitida (M.Sc. Thesis). Universidad de Antioquia, Medellín, Colombia.

Camuffo, D., Becherini, F., della Valle, A., 2020. Relationship between selected percentiles and return periods of extreme events. Acta Geophys. 68 (4), 1201–1211. http://dx.doi.org/10.1007/s11600-020-00452-x.

Carr, D.B., 2003. Graphics in the Physical Sciences. Elsevier, pp. 1–14. http://dx.doi.org/10.1016/B0-12-227410-5/00297-0.

Chavez, S.P., Takahashi, K., 2017. Orographic rainfall hot spots in the andes-amazon transition according to the TRMM precipitation radar and in situ data. J. Geophys. Res.: Atmos. 122, 5870–5882. http://dx.doi.org/10.1002/2016JD026282.

Dafis, S., Lagouvardos, K., Kotroni, V., Giannaros, T.M., Bartzokas, A., 2017. Observational and modeling study of a mesoscale convective system during the HyMeX — SOP1. Atmos. Res. 187, 1–15. http://dx.doi.org/10.1016/j.atmosres.2016.12.001.

Dave, H., M.E., J., 2017. Characteristics of intense rainfall over gujarat state (India) based on percentile criteria. Hydrol. Sci. J. 62 (12), 2035–2048. http://dx.doi.org/10.1080/02626667.2017.1357818.

Dominguez, F., Rasmussen, R., Liu, C., Ikeda, K., Prein, A., Varble, A., Arias, P.A., Bacmeister, J., Bettolli, M.L., Callaghan, P., Carvalho, L.M.V., Castro, C.L., Chen, F., Chug, D., Chun, K.P.S., Dai, A., Danaila, L., da Rocha, R.P., Nascimento, E.d., Dougherty, E., Dudhia, J., Eidhammer, T., Feng, Z., Fita, L., Fu, R., Giles, J., Gilmour, H., Halladay, K., Huang, Y., Iza-Wong, A.M., niga, M.Á.L.-Z., Jones, C., Llamocca, J., Llopart, M., Martinez, J.A., Martinez, J.C., Minder, J.R., Morrison, M., Moon, Z.L., Mu, Y., Neale, R.B., nez Ocasio, K.M.N., Pal, S., Potter, E., Poveda, G., Puhales, F., Rasmussen, K.L., Rehbein, A., Rios-Berrios, R., Risanto, C.B., Rosales, A., Scaff, L., Seimon, A., Somos-Valenzuela, M., Tian, Y., Oevelen, P.V., Veloso-Aguila, D., Xue, L., Schneider, T., 2024. Advancing south American water and climate science through multidecadal convection-permitting modeling. Bull. Am. Meteorol. Soc. 105 (1), E32 – E44. http://dx.doi.org/10.1175/BAMS-D-22-0226.1, URL: https://journals.ametsoc.org/view/journals/bams/105/1/BAMS-D-22-0226.1.xml.

Eldardiry, H., Habib, E., 2020. Examining the robustness of a Spatial Bootstrap Regional approach for radar-based hourly precipitation frequency analysis. Remote. Sens. 12, 3767. http://dx.doi.org/10.3390/rs12223767.

Espinoza, J.C., Chavez, S., Ronchail, J., Junquas, C., Takahashi, K., Lavado, W., 2015. Rainfall hotspots over the southern tropical andes: Spatial distribution, rainfall intensity, and relations with large-scale atmospheric circulation. Water Resour. Res. 51, 3459–3475. http://dx.doi.org/10.1002/2014WR016273.

Gómez-Ríos, S., Zuluaga, M.D., Hoyos, C.D., 2019. Orographic control over convection in an Inter-Andean Valley in Northern South America (M.Sc. Thesis). Universidad Nacional de Colombia, Medellín Colombia.

Gomez-Rios, S., Zuluaga, M.D., Hoyos, C.D., 2023. Orographic controls over convection in an inter-andean valley in Northern South America. Mon. Weather Rev. 151, 145–162. http://dx.doi.org/10.1175/MWR-D-21-0231.1.

Hernandez, K.S., Gomez-Rios, S., Henao, J.J., Robledo, V., Ramirez-Cardona, A., Rendón, A.M., 2024. Rainfall sensitivity to microphysics and planetary boundary layer parameterizations in convection-permitting simulations over Northwestern South America. J. Meteorol. Res. 38 (4), 1–20. http://dx.doi.org/10.1007/s13351-024-3156-4.

Hernandez-Deckers, D., 2022. Features of atmospheric deep convection in northwestern south america obtained from infrared satellite data. Q. J. R. Meteorol. Soc. 148, 338–350. http://dx.doi.org/10.1002/qj.4208.

Hersbach, H., Bell, B., Berrisford, P., Biavati, G., Horányi, A., Sabater, J.M., Nicolas, J., Peubey, C., Radu, R., Rozum, I., Schepers, D., Simmons, A., Soci, C., Dee, D., Thépaut, J.-N., 2023. ERA5 hourly data on single levels from 1940 to present. http://dx.doi.org/10.24381/cds.adbb2d47, URL: https://cds.climate.copernicus.eu/cdsapp{#}!/dataset/10.24381/cds.adbb2d47?tab=overview.

Hoyos, C.D., Ceballos, L.I., Pérez-Carrasquilla, J.S., Sepúlveda, J., López-Zapata, S.M., Zuluaga, M.D., Velásquez, N., Herrera-Mejía, L., Hernández, O., Guzmán-Echavarría, G., Zapata, M., 2019. Meteorological conditions leading to the 2015 salgar flash flood: lessons for vulnerable regions in tropical complex terrain. Nat. Hazards Earth Syst. Sci. 19, 2635–2665. http://dx.doi.org/10.5194/nhess-19-2635-2019.

Hu, X., Yuan, W., 2021. Evaluation of ERA5 precipitation over the eastern periphery of the tibetan plateau from the perspective of regional rainfall events. Int. J. Climatol. 41, 2625–2637. http://dx.doi.org/10.1002/joc.6980.

Huang, J., Sun, S., Xue, Y., Li, J., Zhang, J., 2014. Spatial and temporal variability of precipitation and dryness/wetness during 1961–2008 in Sichuan Province, west China. Water Resour. Manag. 28, 1655–1670. http://dx.doi.org/10.1007/s11269-014-0572-8.

Junquas, C., Takahashi, K., Condom, T., Espinoza, J.-C., Chavez, S., Sicart, J.-E., Lebel, T., 2018. Understanding the influence of orography on the precipitation diurnal cycle and the associated atmospheric processes in the central andes. Clim. Dyn. 50, 3995–4017. http://dx.doi.org/10.1007/s00382-017-3858-8.

Kara, G.T., Elbir, T., 2025. Seasonal and spatial variability in the accuracy of hourly ERA5 and MERRA-2 reanalysis datasets: A 14-year comparison with observed meteorological data in Türkiye. Atmos. Res. 325, 108233. http://dx.doi.org/10.1016/j.atmosres.2025.108233.

Kuswanto, H., Andari, S., Permatasari, E.O., 2015. Identification of extreme events in climate data from multiple sites. Procedia Eng. 125, 304–310. http://dx.doi.org/10.1016/j.proeng.2015.11.067.

Lengfeld, K., Kirstetter, P.-E., Fowler, H.J., Yu, J., Becker, A., Flamig, Z., Gourley, J., 2020. Use of radar data for characterizing extreme precipitation at fine scales and short durations. Environ. Res. Lett. 15, 085003. http://dx.doi.org/10.1088/1748-9326/ab98b4.

Liu, N., Liu, C., Chen, B., Zipser, E., 2020. What are the favorable large-scale environments for the highest-flash-rate thunderstorms on earth? J. Atmos. Sci. 77 (5), 1583–1612.

Liu, Q., Yang, Z., Cui, B., 2008. Spatial and temporal variability of annual precipitation during 1961–2006 in yellow river Basin, China. J. Hydrol. 361, 330–338. http://dx.doi.org/10.1016/j.jhydrol.2008.08.002.

Marra, F., Armon, M., Morin, E., 2022. Coastal and orographic effects on extreme precipitation revealed by weather radar observations. Hydrol. Earth Syst. Sci. 26, 1439–1458. http://dx.doi.org/10.5194/hess-26-1439-2022.

Martinez, J.A., Arias, P.A., Dominguez, F., Prein, A., 2024. Mesoscale structures in the orinoco basin during an extreme precipitation event in the tropical Andes. Front. Earth Sci. 11, http://dx.doi.org/10.3389/feart.2023.1307549.

May, W., 2004. Variability and extremes of daily rainfall during the Indian summer monsoon in the period 1901–1989. Glob. Planet. Change 44 (1), 83–105. http://dx.doi.org/10.1016/j.gloplacha.2004.06.007, Extreme climatic events.

Mejía, J.F., Yepes, J., Henao, J.J., Poveda, G., Zuluaga, M.D., Raymond, D.J., Fuchs-Stone, Ž., 2021. Towards a mechanistic understanding of precipitation over the far eastern tropical Pacific and western Colombia, one of the rainiest spots on earth. J. Geophys. Res.: Atmos. 126 (5), e2020JD033415.

Meshram, S.G., Singh, V.P., Meshram, C., 2017. Long-term trend and variability of precipitation in Chhattisgarh state, India. Theor. Appl. Climatol. 129, 729–744. http://dx.doi.org/10.1007/s00704-016-1804-z.

Mutlu, A., 2025. Comparative evaluation of NASA, ERA5, and observational data for accuracy and reliability. Theor. Appl. Climatol. 156, http://dx.doi.org/10.1007/s00704-025-05605-w.

Oster, R., 1979. Las precipitaciones en Colombia. Colombia Geográfica, Instituto Agusín Codazzi.

Overeem, A., Buishand, T.A., Holleman, I., 2009. Extreme rainfall analysis and estimation of depth-duration-frequency curves using weather radar. Water Resour. Res. 45, http://dx.doi.org/10.1029/2009WR007869.

Peleg, N., Marra, F., Fatichi, S., Paschalis, A., Molnar, P., Burlando, P., 2018. Spatial variability of extreme rainfall at radar subpixel scale. J. Hydrol. 556, 922–933. http://dx.doi.org/10.1016/j.jhydrol.2016.05.033.

Peters, J.M., Schumacher, R.S., 2015. Mechanisms for organization and echo training in a flash-flood-producing mesoscale convective system. Mon. Weather Rev. 143, 1058–1085. http://dx.doi.org/10.1175/MWR-D-14-00070.1.

Poveda, G., Espinoza, J.C., Zuluaga, M.D., Solman, S.A., Garreaud, R., van Oevelen, P.J., 2020. High impact weather events in the andes. Front. Earth Sci. 8, http://dx.doi.org/10.3389/feart.2020.00162.

Poveda, G., Mesa, O.J., Salazar, L.F., Arias, P.A., Moreno, H.A., Vieira, S.C., Agudelo, P.A., Toro, V.G., Alvarez, J.F., 2005. The diurnal cycle of precipitation in the tropical andes of Colombia. Mon. Weather Rev. 133, 228–240. http://dx.doi.org/10.1175/MWR-2853.1.

Raja, N.B., Aydin, O., Türkoğlu, N., Çiçek, I., 2017. Space-time kriging of precipitation variability in Turkey for the period 1976–2010. Theor. Appl. Climatol. 129, 293–304. http://dx.doi.org/10.1007/s00704-016-1788-8.

Raymond, C., Horton, R.M., Zscheischler, J., Martius, O., AghaKouchak, A., Balch, J., Bowen, S.G., Camargo, S.J., Hess, J., Kornhuber, K., Oppenheimer, M., Ruane, A.C., Wahl, T., White, K., 2020. Understanding and managing connected extreme events. Nat. Clim. Chang. 10, 611–621. http://dx.doi.org/10.1038/s41558-020-0790-4.

Robledo, V., Henao, J.J., Mejía, J.F., Ramírez-Cardona, Á., Hernández, K.S., Gomez-Rios, S., Rendón, Á.M., 2024. Climatological tracking and lifecycle characteristics of mesoscale convective systems in Northwestern South America. J. Geophys. Res.: Atmos. 129 (19), e2024JD041159.

Sang, Y.-F., Wang, Z., Liu, C., 2014. Spatial and temporal variability of precipitation extrema in the haihe river basin, China. Hydrol. Process. 28, 926–932. http://dx.doi.org/10.1002/hyp.9607.

Schär, C., Ban, N., Fischer, E.M., Rajczak, J., Schmidli, J., Frei, C., Giorgi, F., Karl, T.R., Kendon, E.J., Tank, A.M.G.K., O'Gorman, P.A., Sillmann, J., Zhang, X., Zwiers, F.W., 2016. Percentile indices for assessing changes in heavy precipitation events. Clim. Change 137, 201–216. http://dx.doi.org/10.1007/s10584-016-1669-2.

Segura, H., Junquas, C., Espinoza, J.C., Vuille, M., Jauregui, Y.R., Rabatel, A., Condom, T., Lebel, T., 2019. New insights into the rainfall variability in the tropical andes on seasonal and interannual time scales. Clim. Dyn. 53, 405–426. http://dx.doi.org/10.1007/s00382-018-4590-8.

Seidel, J., Trachte, K., Orellana-Alvear, J., Figueroa, R., Célleri, R., Bendix, J., Fernandez, C., Huggel, C., 2019. Precipitation characteristics at two locations in the tropical andes by means of vertically pointing micro-rain radar observations. Remote. Sens. 11, 2985. http://dx.doi.org/10.3390/rs11242985.

Sepulveda, J., 2016. Estimación cuantitativa de precipitación a partir de la información de Radar Meteorológico del Área Metropolitana del Valle de Aburrá. Universidad Nacional de Colombia, URL: https://repositorio.unal.edu.co/handle/unal/58046.

Shi, P., Wu, M., Qu, S., Jiang, P., Qiao, X., Chen, X., Zhou, M., Zhang, Z., 2015. Spatial distribution and temporal trends in precipitation concentration indices for the southwest China. Water Resour. Manag. 29, 3941–3955. http://dx.doi.org/10.1007/s11269-015-1038-3.

Srivastava, N.A., Mascaro, G., 2023. Improving the utility of weather radar for the spatial frequency analysis of extreme precipitation. J. Hydrol. 624, 129902. http://dx.doi.org/10.1016/j.jhydrol.2023.129902.

Stott, P.A., Christidis, N., Otto, F.E.L., Sun, Y., Vanderlinden, J.-P., van Oldenborgh, G.J., Vautard, R., von Storch, H., Walton, P., Yiou, P., Zwiers, F.W., 2016. Attribution of extreme weather and climate-related events. WIREs Clim. Chang. 7, 23–41. http://dx.doi.org/10.1002/wcc.380.

Tao, Y., Wang, W., Song, S., Ma, J., 2018. Spatial and temporal variations of precipitation extremes and seasonality over China from 1961 2013. Water 10, 719. http://dx.doi.org/10.3390/w10060719.

Tongal, H., 2019. Spatiotemporal analysis of precipitation and extreme indices in the antalya Basin, Turkey. Theor. Appl. Climatol. 138, 1735–1754. http://dx.doi.org/10.1007/s00704-019-02927-4.

Urrea, V., Ochoa, A., Mesa, O., 2019. Seasonality of rainfall in Colombia. Water Resour. Res. 55, 4149–4162. http://dx.doi.org/10.1029/2018WR023316.

Vásquez-Franco, D.F., Arias, P., Martinez, J., 2023. Diagnóstico de las condiciones atmosféricas asociadas a eventos intensos de precipitación sobre el suroeste de Colombia (M.Sc. Thesis). Universidad Nacional de Colombia, Medellín Colombia.

Vega, J., Barco, J., Hidalgo, C., 2024. Space-time analysis of the relationship between landslides occurrence, rainfall variability and ENSO in the tropical andean mountain region in Colombia. Landslides 21, 1293–1314. http://dx.doi.org/10.1007/s10346-024-02225-9.

Velásquez, N., 2022. Assessment of deep convective systems in the Colombian andean region. Hydrology 9, 119. http://dx.doi.org/10.3390/hydrology9070119.

Villalobos-Puma, E., Morales, A., Martinez-Castro, D., Valdivia, J., Cardenas-Vigo, R., Lavado-Casimiro, W., Santiago, A., 2024. Dynamic atmospheric mechanisms associated with the diurnal cycle of hydrometeors and precipitation in the Andes–Amazon transition zone of central Peru during the summer season. J. Earth Syst. Sci. 133, 75. http://dx.doi.org/10.1007/s12040-024-02278-3, URL: https://link.springer.com/10.1007/s12040-024-02278-3.

Villarini, G., Smith, J.A., Baeck, M.L., Sturdevant-Rees, P., Krajewski, W.F., 2010. Radar analyses of extreme rainfall and flooding in urban drainage basins. J. Hydrol. 381, 266–286. http://dx.doi.org/10.1016/j.jhydrol.2009.11.048.

Warner, T.T., Mapes, B.E., Xu, M., 2003. Diurnal patterns of rainfall in northwestern South America. Part II: Model simulations. Mon. Weather Rev. 131, 813–829. http://dx.doi.org/10.1175/1520-0493(2003)131<0813:DPORIN>2.0.CO;2.

Wei, Y., Sun, Y., Ma, Y., Tan, Y., Ren, X., Peng, K., Yang, S., Lin, Z., Zhou, X., Ren, Y., Ahmed, M., Tian, Y., Xin, J., 2025. Deviations of boundary layer height and meteorological parameters between ground-based remote sensing and ERA5 over the complex terrain of the mongolian plateau. Remote. Sens. 17, http://dx.doi.org/10.3390/rs17030393.

Wright, D.B., Smith, J.A., Villarini, G., Baeck, M.L., 2013. Estimating the frequency of extreme rainfall using weather radar and stochastic storm transposition. J. Hydrol. 488, 150–165. http://dx.doi.org/10.1016/j.jhydrol.2013.03.003.

Yepes, J., Mejía, J.F., Mapes, B., Poveda, G., 2020. Gravity waves and other mechanisms modulating the diurnal precipitation over one of the rainiest spots on earth: Observations and simulations in 2016. Mon. Weather Rev. 148 (9), 3933–3950.

Yepes, J., Poveda, G., Mejía, J.F., Moreno, L., Rueda, C., 2019. Choco-jex: A research experiment focused on the Chocó low-level jet over the far eastern Pacific and western Colombia. Bull. Am. Meteorol. Soc. 100 (5), 779–796.

Zoccatelli, D., Borga, M., Viglione, A., Chirico, G.B., Blöschl, G., 2011. Spatial moments of catchment rainfall: rainfall spatial organisation, basin morphology, and flood response. Hydrol. Earth Syst. Sci. 15, 3767–3783. http://dx.doi.org/10.5194/hess-15-3767-2011.

Zuluaga, M.D., Houze, R.A., 2015. Extreme convection of the near-equatorial Americas, Africa, and adjoining oceans as seen by TRMM. Mon. Weather Rev. 143, 298–316. http://dx.doi.org/10.1175/MWR-D-14-00109.1.

Zwiers, F.W., Alexander, L.V., Hegerl, G.C., Knutson, T.R., Kossin, J.P., Naveau, P., Nicholls, N., Schär, C., Seneviratne, S.I., Zhang, X., 2013. Climate extremes: Challenges in estimating and understanding recent changes in the frequency and intensity of extreme climate and weather events. In: Climate Science for Serving Society. Springer Netherlands, Dordrecht, pp. 339–389. http://dx.doi.org/10.1007/978-94-007-6692-1_13.

Atmospheric Research

COUNTRY	SUBJECT AREA AND CATEGORY	PUBLISHER	SJR 2024
Netherlands Universities and research institutions in Netherlands Media Ranking in Netherlands	Earth and Planetary Sciences Atmospheric Science	Elsevier B.V.	1.440 Q1 H-INDEX 148

PUBLICATION TYPE	ISSN	COVERAGE	INFORMATION
Journals	01698095	1986-2025	Homepage How to publish in this journal Contact

SCOPE

The journal publishes scientific papers (research papers, review articles, letters and notes) dealing with the part of the atmosphere where meteorological events occur. Attention is given to all processes extending from the earth surface to the tropopause, but special emphasis continues to be devoted to the physics of clouds, mesoscale meteorology and air pollution, i.e. atmospheric aerosols; microphysical processes; cloud dynamics and thermodynamics; numerical simulation, climatology, climate change and weather modification.

Join the conversation about this journal

Quartiles

FIND SIMILAR JOURNALS

1
Asia-Pacific Journal of Atmospheric Sciences
KOR
82%
similarity

2
Atmosfera
MEX
80%
similarity

3
Journal of Geophysical Research: Atmospheres
USA
78%
similarity

4
Plateau Meteoro
CHN
75
simila

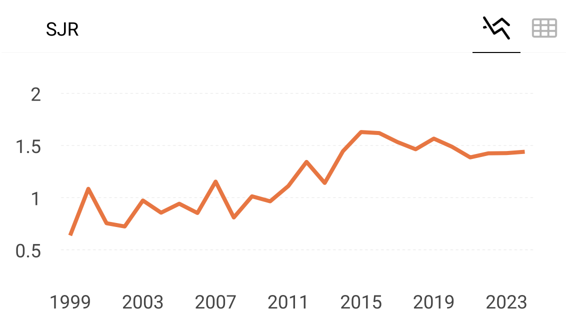

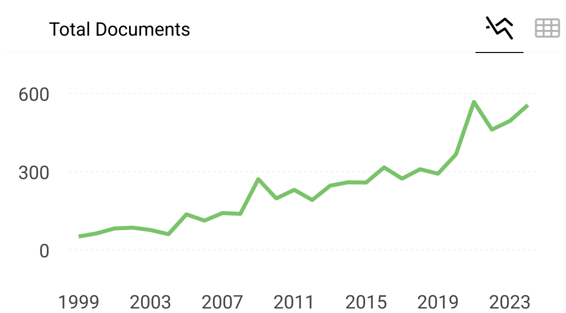

Total Cites Self-Cites

Citations per document

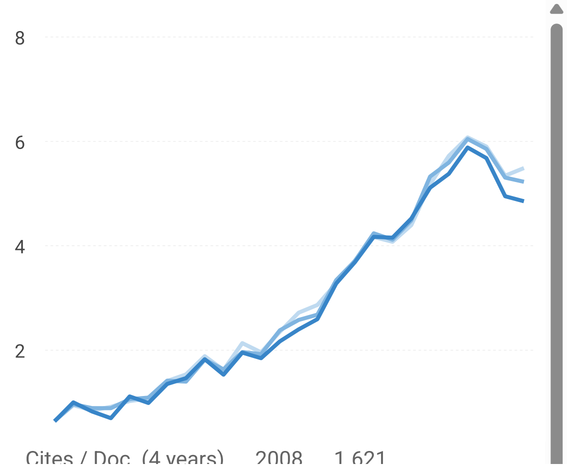

External Cites per Doc Cites per Doc

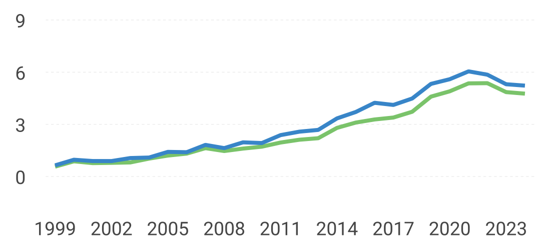

% International Collaboration

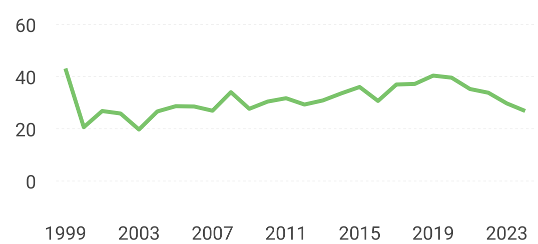

Citable documents Non-citable documents

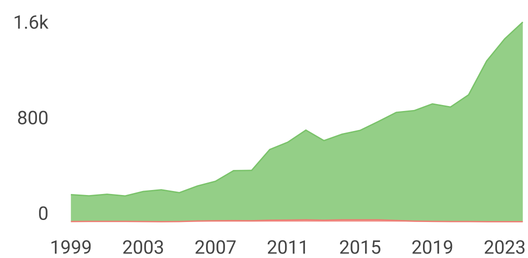

Cited documents Uncited documents

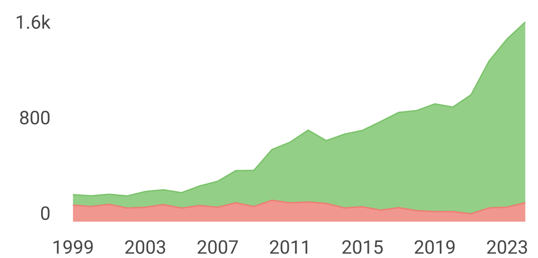

% Female Authors

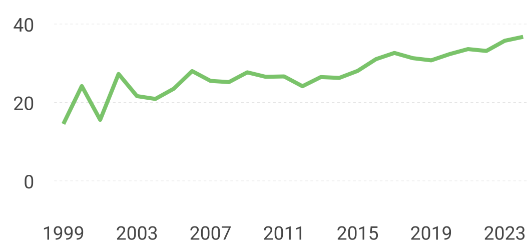

Documents cited by public policy (Overton)

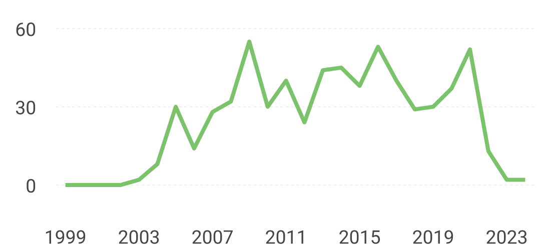

Documents related to SDGs (UN)

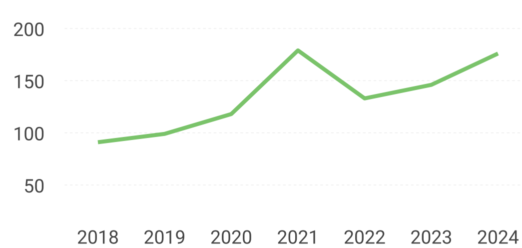

Estimated APC

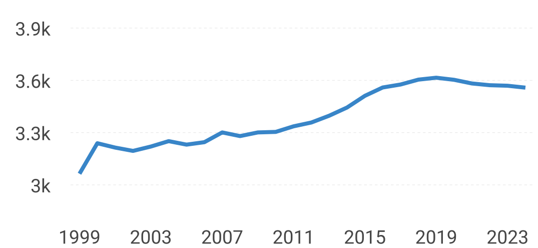

Estimated financial value

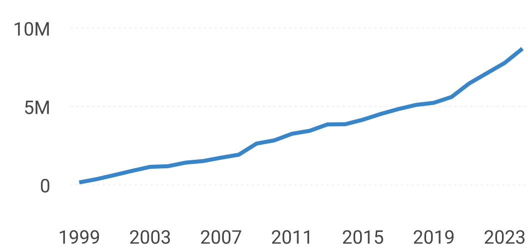

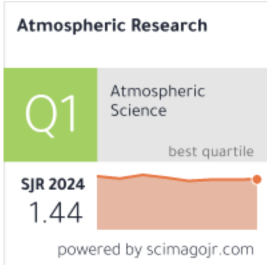

← Show this widget in your own website

Just copy the code below and paste within your html code:

<a href="https://www.scimag

SCImago Graphica

Explore, visually communicate and make sense of data with our **new data visualization tool**.

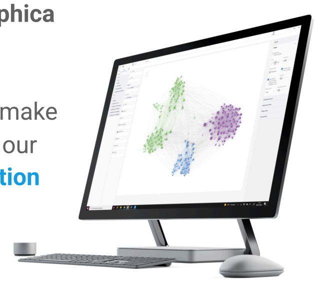

Metrics based on Scopus® data as of March 2025

Loading comments...

Developed by: SCImago

Powered by: Scopus